Large-Area Oblique-Aligned ZnO Nanowires through a Continuously Bent Columnar Buffer: Growth, Microstructure, and Antireflection

ARTICLE *in* CRYSTAL GROWTH & DESIGN · JULY 2010

Impact Factor: 4.89 · DOI: 10.1021/cg901506v

7 AUTHORS, INCLUDING:

Cheng-Ying Chen
National Taiwan University
44 PUBLICATIONS **853** CITATIONS

SEE PROFILE

Chuan-Pu Liu
National Cheng Kung University
248 PUBLICATIONS **3,240** CITATIONS

SEE PROFILE

DOI: 10.1021/cg901506v

CRYSTAL GROWTH & DESIGN
Communication
2010, Vol. 10
3297–3301

Large-Area Oblique-Aligned ZnO Nanowires through a Continuously Bent Columnar Buffer: Growth, Microstructure, and Antireflection

Jun-Han Huang,[†] Cheng-Ying Chen,[‡] Yi-Feng Lai,[†] Yu-I Shih,[†] Yuh-Chieh Lin,[†] Jr-Hau He,[‡] and Chuan-Pu Liu*,[†]

[†]*Department of Materials Science and Engineering, National Cheng Kung University, Tainan 701, Taiwan, Republic of China, and* [‡]*Institute of Photonics and Optoelectronics, and Department of Electrical Engineering, National Taiwan University, Taipei 10617, Taiwan, Republic of China*

Received December 8, 2009; Revised Manuscript Received June 19, 2010

ABSTRACT: We demonstrate a novel defect-induced bending mechanism for a modified oblique-angle deposition (OAD) system, where different defect density was introduced to accommodate the mass difference between the shadowed and exposed surfaces, leading to continuous structural bending. Oblique angle sputtering and hydrothermal processes were employed for growth of inclined ZnO nanowire arrays on ZnO bent columns. Transmission electron microscopy images reveal that a dislocation network was introduced to accommodate the mass difference in bent columns, and the bending angle could be controlled by growth temperature. Nanowires were then grown along the tangent lines of the bent column tips. The bent column curvature and limited space determine the nanowire growth direction. The reflectance measurements demonstrate that the oblique-aligned ZnO nanowire arrays are an excellent candidate for antireflection coatings, showing the significant suppression of reflectance of 87.5% and 90.0% for polished Si under TE and TM polarization, respectively. The interference oscillations of reflectance show the optical anisotropy of oblique-aligned ZnO nanowire arrays, which is dependent on the angle range of nanowire direction.

First discovered in 1959,[1,2] oblique-angle deposition (OAD) has since developed well and become a technique to grow anisotropic nanostructure. Moreover, in the recent two decades, more hierarchical nanostructures into three-dimensions have been developed based on the OAD-related technology, such as helical,[3−5] direction and symmetry control,[6,7] and branched structures.[8−10] The control over the direction of the growth front of nanostructures provides an additional degree of freedom to design for complex nanostructures, thus enabling applications in new fields, such as hydrogen or energy storage,[11,12] mechanical or biological sensors,[13,14] mechanical components,[15] field emissions,[16] photonic crystals,[17,18] enhanced birefringence,[19] enhanced light extraction of light emitting diodes,[20] and antireflection for solar cells.[21,22] However, the OAD technology usually grows poor crystallinity of the nanostructures and allows a limited range of the nanowire growth direction, which represent the major weaknesses of the technology for some applications, especially in optoelectronic devices.

The OAD deposited nanostructures usually grew toward the incident source direction via a shadowing effect and limited adatom diffusion.[23,24] Therefore, most OAD experiments were requested to operate at low energetic growth conditions, so that adatoms can merely migrate a short distance by shadowing. That is the reason why the nanostructures were aligned only with the incident source direction and usually grew in poor crystal quality. The oblique angle of the grown nanostructures relative to the substrate surface normal is far smaller than the incident flux angle, following the common predictions from the experimental tangent rule[25] or the theoretical Tait's rule.[26]

So far, only a few reports have obtained oblique structures with good crystallinity.[27,28] To achieve oblique nanowire arrays aligned in an even larger range of angles with single crystallinity is apparently very challenging, though the breakthrough can lead to expanding the potential applications into optoelectronic devices. On the other hand, emerging nanofabrication technology has enabled materials to be engineered to meet desired antireflection (AR) characteristics,[29] however through complicated procedures. Very recently, ZnO nanostructures were shown to bring exciting possibilities for next-generation AR coatings (ARCs) to suppress the Fresnel reflection effectively.[30] In this report, we demonstrate an interesting approach by a combined method of modified OAD and hydrothermal growth to grow oblique ZnO nanowire arrays at any angle with single crystallinity, whose growth mechanism differs from the typical OAD. Furthermore, reflectance measurements have been examined to demonstrate the oblique-aligned ZnO nanowire arrays as an excellent ARC for photovoltaic application. The correlation between the oblique angle of nanowires and reflectance has been discussed. This growth mechanism is universal and can be applied to other materials for more applications, in principle.

An oblique-angle sputter system followed by hydrothermal growth was used to grow a direction-controlled ZnO nanowire array on Si(100). A pure ZnO target (99.99%) was used as the sputtering source. At first, a thin ZnO buffer with *c*-axis vertically aligned was deposited at a 30° oblique angle with 1 rpm substrate rotation in argon at 410 °C. Subsequently, a layer with bent columns was designed on the buffer in a reduced atmosphere with 20% hydrogen/argon mixture gas; with the oblique angle, α, set at 30° relative to the surface normal, no substrate rotation was applied during this step. Three growth temperatures were attempted, which were 460 °C, 320 °C, and 265 °C. For the final hydrothermal process, the samples were grown in a solution of 0.005 M zinc acetate dehydrate ($Zn(CH_3COO)_2 \cdot 2H_2O$) and 0.005 M hexamethylenetetramine (HMT $C_6H_{12}N_4$) in the ratio of 1:1, heated at 81 °C for 2 h. TEM samples were prepared with a SMI 3050 focused ion beam (FIB). JEOL-7000 field-emission scanning electron microscopy (SEM) was operated at 10 keV to image nanostructure morphology. JEOL-2100F field-emission transmission electron microscopy (TEM) at 200 keV and X-ray diffraction (XRD) spectroscopy were employed to characterize the microstructure. Optical reflectance measurements were performed at the angle of incidence (AOI) of 8° for TE and TM polarization in the wavelength ranges of 200 to 850 nm with a standard UV−vis-NIR spectrophotometer (JASCO V-670). The reflection of a collimated incident light beam was measured by collecting the specularly reflected cone of light within an acceptance angle of 8°.

*Corresponding author. E-mail:cpliu@mail.ncku.edu.tw. Telephone: 886-6-2757575-62943. Fax: 886-6-2346290.

Published on Web 07/12/2010

Figure 1 shows the ZnO buffers by oblique sputter deposition and oblique-aligned nanowires by subsequent hydrothermal growth for different growth conditions, with white arrows indicating the major incident flux direction. The bent columns grown at different temperatures are compared between 265 and 320 °C in Figure 1. When grown at 265 °C, due to a lower temperature and hydrogen reduction rate, the as-grown columns are thicker with a smoother surface. Some grains even grew laterally and could be observed clearly in Figure 1a. When grown at 320 °C, two kinds of structures are present, including bent columns and pyramidal grains, as indicated in Figure 1c. The ZnO oblique nanowire arrays, as shown in Figure 1b and d, are grown on the templates as shown in Figure 1a and c, respectively. Both scanning electron microscopy (SEM) images have demonstrated the successful growth of nanowire arrays inclined at different angles determined by the growth temperature of the buffer, but still with a few nanowires grown into different angle ranges from the majority, possibly due to the presence of the pyramidal grains.

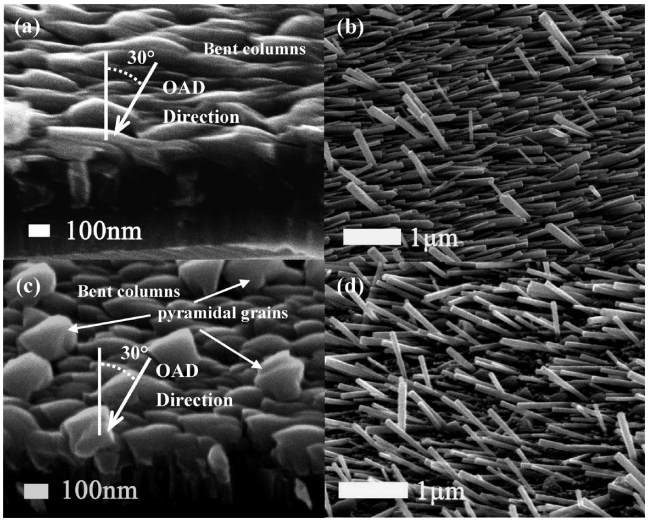

Figure 1. Tilted-view SEM images of the ZnO bent columns and nanowires: (a) columns grown at 265 °C with incident flux angle set at 30°; (b) ZnO nanowires by hydrothermal process on the columns in part a; (c) columns grown at 320 °C with incident flux angle set at 30°; (d) ZnO nanowires by hydrothermal process on the columns in part c.

Figure 2a shows the transmission electron microscopy (TEM) bright-field cross-sectional image of the bent columns grown at 320 °C with a ZnO buffer below and a nanowire above. It can be seen clearly that the column bends continuously away from the incident flux direction upon oblique-angle deposition. Selected area diffraction patterns (SADP) in Figure 2b and c reveal that the first-step buffer is composed of columnar grains with the *C*-axis vertical to the substrate; however, individual columns in the second-step buffer are characterized by arcs instead of spots in the SADP, confirming the continuous column bending in a wide range of angle of about 18°. The high-resolution TEM (HRTEM) image in Figure 2d reveals that the lattice-bending phenomenon is accommodated by dislocation networks, where the exposed side on the left contains more dislocations than the shadowed side on the right, leading to the columns bending to the shadowed side continuously. No grain boundaries and twin grains in the whole column suggests that the major bending mechanism is dominated by dislocations. The HRTEM image in Figure 2e clearly shows that the nanowire nucleates at the exposed side of the bent column. The direction of the ZnO (0002) of both the nanowire and the column is the same at the nucleation site but splits into two slightly different directions as the nanowire proceeded with

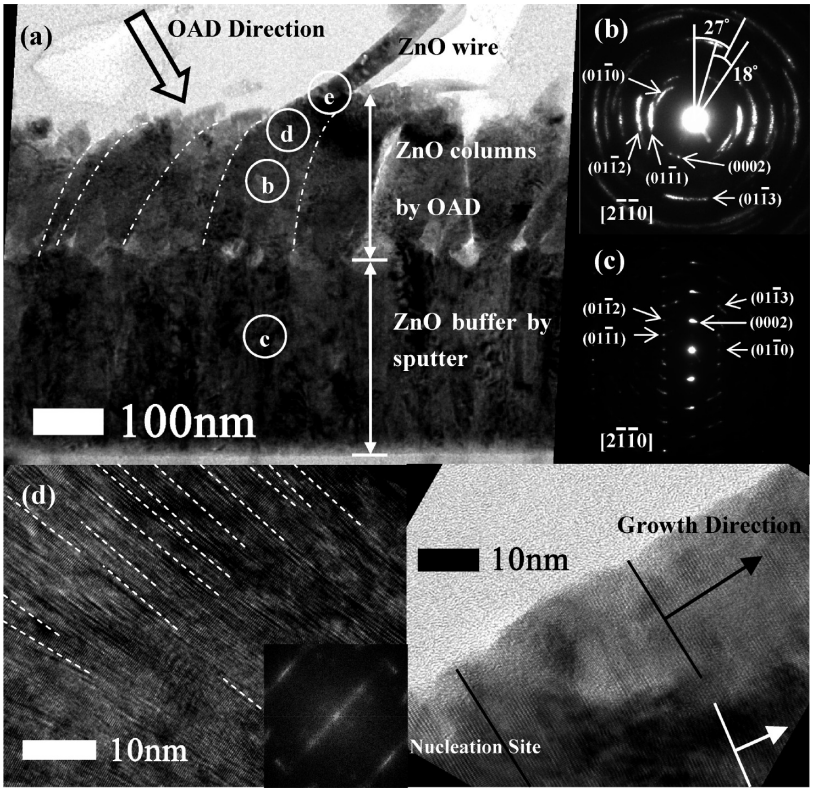

Figure 2. (a) TEM cross-sectional bright-field image of the ZnO bent columns grown at 320 °C with a nanowire, where the DPs in parts b and c are taken from the bent columns and buffer, respectively, as marked in part a, and the HRTEM images in parts d and e represent the bent column and the interface between the ZnO nanowire and column, respectively, as marked in part a. The inset in part d is the corresponding DP by Fourier transformation.

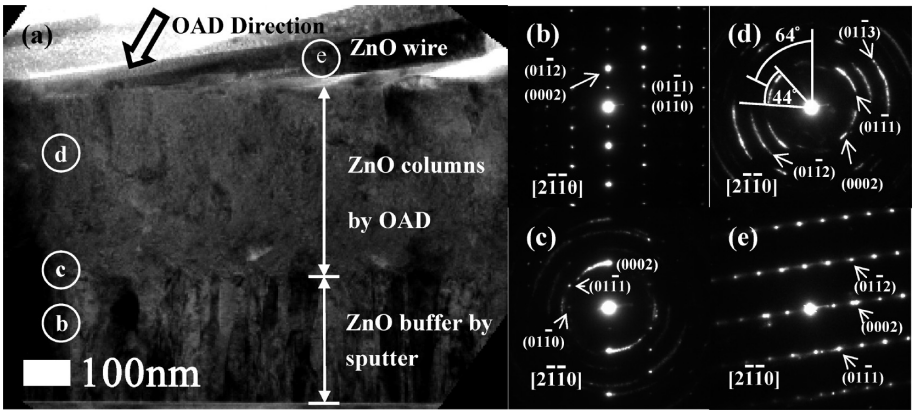

Figure 3. (a) TEM cross-sectional bright-field image of the ZnO bent columns grown at 265 °C with a nanowire, with the SADPs in parts b−e corresponding to the area marked in part a. From part d, ZnO(0002) varied in a wide angle range of 44° with an average incline angle of 64° to the substrate normal.

Table 1. Important Parameters and Results Extracted from Samples

growth temp (°C)	avg column lateral size (nm)	column growth rate (nm/min)	bending rate (deg/nm)	NWs angle range[a] (°C)	NWs direction to OAD source
265	grain boundary indistinct	3.41	0.32	60−80	partially backward
320	80	2.4	0.27	30−70	forward
460[b]	120	1.31	no bending		

[a] Angle between NW and substrate normal. [b] Three-steps grown columns, as shown in Supporting Information Figure S1.

further growth. This indicates the column surface was curved, and the nanowire grew along the tangent line of the nucleation area.

Figure 3 shows the TEM results of the morphology for the template layer grown at 265 °C. As shown in Figure 3a, the columnar layer is thicker due to a higher growth rate and the column boundaries become indistinct. According to the SADPs in Figure 3b−e, taken from the area as marked in Figure 3a, the ZnO(0002) columns almost bent horizontally to the substrate normal, resulting in the nanowires being nucleated and grown backward compared to the bending direction.

Table 1 summarizes the important results extracted from the three samples, including average column size, normal growth rate and bending rate of the columns, and growth direction and angle of nanowires, all exhibiting strong dependence on growth temperature.

Our results suggest that the growth mechanism responsible for the modified OAD deposition with higher adatom energy employed here must be distinct from any existing models. We suggest that both higher surface diffusion and reduction reaction of ZnO with hydrogen improve the crystal quality and control the degree of bending through growth temperature. For the highest temperature in this experiment at 460 °C (shown in Supporting Information Figure S1), even merely slight tilting in morphology without crystal reorientation is observed. However, for lower growth temperatures, the shadowing effect becomes more important due to shorter diffusion lengths.[23,24] Correspondingly, dislocations were introduced in the exposed area to accommodate the mass difference, and the structures started to bend in the opposite direction, rather than bending toward the incident source, causing nanostructure bending both morphologically and crystallographically. The XRD spectra of the ZnO buffers deposited with sample rotation (by pure Ar) and oblique deposition with no rotation (by H_2/Ar mixture gas) at different temperatures, as shown in Supporting Information Figure S2, exhibit single crystalline behavior with only ZnO(0002), ZnO(0004), and Si(400) peaks. Figure 4 compares the enlarged ZnO(0002) peak from the XRD results of these three films by normalizing Si(400). Compared with the normal ZnO buffer, the ZnO columns with the modified OAD deposition exhibit dramatically reduced

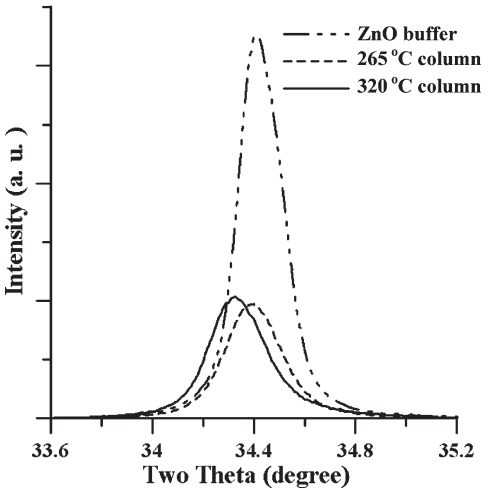

Figure 4. Enlarged ZnO(0002) peak of XRD spectra of the ZnO buffers deposited with sample rotation (by pure Ar) and oblique deposition with no rotation (by H_2/Ar mixture gas) at different temperatures.

(0002) peak intensity and broadened full width at half-maximum. These clearly indicate that the growth direction of the columns deviates from (0002) and more lattice distortion is involved, which strongly supports the SEM and TEM results for the growth mechanism. In addition, the (0002) peak from the one grown at 320 °C shifts to lower angle, indicative of an even larger lattice constant. This defect-induced bending mechanism has not been observed and discussed in earlier OAD related papers, and the nanostructure growth direction cannot be predicted by both tangent and Tait's rule.

Based on the aforementioned mechanism and experimental results, ZnO column tips are eventually directed upward or downward by controlling the degree of column bending through defect density engineering when deposited at different temperature. Subsequently, the resulting inclined ZnO nanowires of various angles by hydrothermal processes were obtained in the

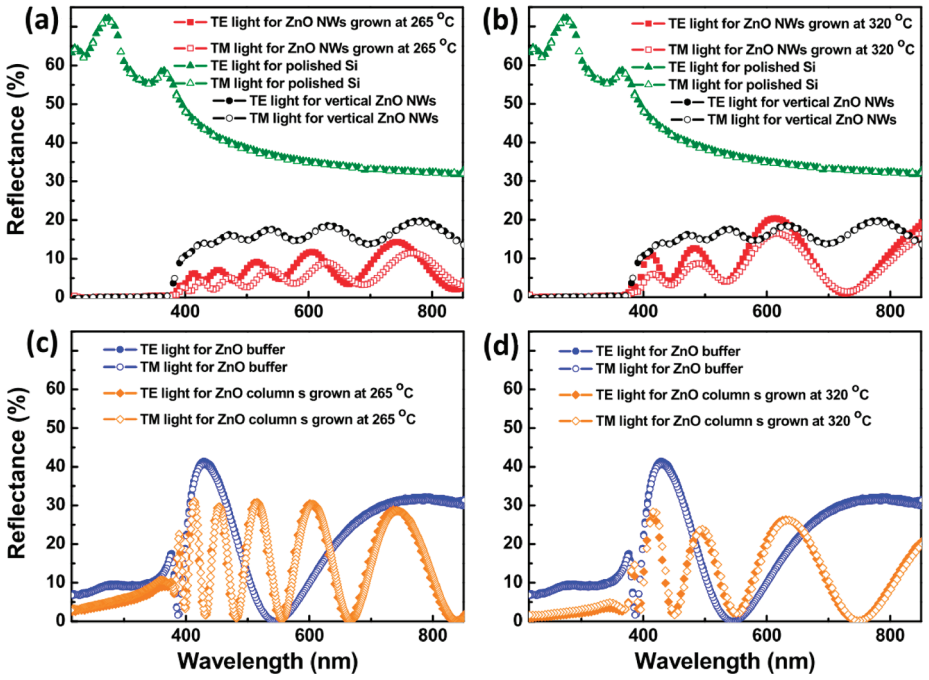

Figure 5. Reflectance spectra of polished silicon: the vertical-aligned and oblique-aligned ZnO nanowires grown at (a) 265 °C and (b) 320 °C and the ZnO bent columns grown at (c) 265 °C and (d) 320 °C for TE and TM polarization.

second-step growth by extending the tangent lines of the curved column tips. Besides the tip curvature, the column spacing also affects the nanowire growth direction. Neighboring columns would limit each other with regard to the direction that nanowire can spread. With tip curvature and neighboring column confinement combined, only some particular directions are allowed for nanowire growth. This concept can better explain why the nanowires spread into an entirely opposite direction with different tip curvature, as shown in Figures 2 and 3, which are also sketched in Figure S3.

In order to investigate the reflective optical properties of the whole oblique-aligned ZnO nanowire arrays, the reflectance measurements were performed at the angle of incidence (AOI) of 8° for TE and TM polarization in the wavelength ranges of 200 to 850 nm, as shown in Figure 5a and b, inclusive of a bare Si and a similar sample with vertical-aligned nanowire arrays for comparison. In this measurement, the electric fields of light are perpendicular and parallel to the nanowires of arrays for TE and TM polarized lights, respectively. When the incident photon energy is larger than the direct band gap energy of ZnO (λ < 368 nm), the reflectance is related with band-gap absorption, leading to flat and ultralow reflectance spectra for TE and TM lights. When the incident photon energy is below the band-gap energy of ZnO (λ > 368 nm), observed AR characteristics can be correlated with the structural properties instead of band-gap absorption. All Si substrates with the oblique-aligned ZnO nanowires exhibit significantly low reflectance spectra over a wide range of wavelengths, as compared with polished Si or even the vertical-aligned nanowires, demonstrating its broad-band AR characteristics. In addition, the reflectance reveals interference oscillations due to the effect of Fabry−Pérot cavities.

To further investigate the AR characteristics of the whole ZnO nanowire arrays structure, we also performed reflectance measurements on the ZnO columns/buffer/Si and the ZnO buffer/Si samples for TE and TM polarizations, as shown in Figure 5c and d. The flatter spectra due to the band-gap absorption and the oscillated spectra due to the effect of Fabry−Pérot cavities are also observed in these reflectance spectra. Because the refractive index of ZnO is smaller than that of silicon, the optical reflectance is reduced as compared with that of Si substrate after depositing

Table 2. Wavelength-Averaged Reflectance (R_{avg}) and Suppression of Reflectance after Growth of a ZnO Buffer Film, ZnO Columns, and Vertical-Aligned and Oblique-Aligned ZnO Nanowires

	R_{avg} (%)		suppressed R_{avg} over Si (%)	
	TE	TM	TE	TM
bare Si substrate	43.2	43.0		
ZnO buffer film	19.1	18.5	55.8	57.0
ZnO columns grown at 265 °C	12.9	13.2	70.1	69.3
ZnO columns grown at 320 °C	10.1	10.4	76.6	75.8
vertical-aligned ZnO nanowires	11.8	11.6	72.7	73.0
ZnO nanowires grown at 265 °C	5.4	4.3	87.5	90.0
ZnO nanowires grown at 320 °C	7.3	5.8	83.1	86.5

the buffer film and the columns. In addition, it is worth noting that the optical reflectance is further decreased after the growth of the oblique-aligned ZnO nanowires, indicating that the nanowires play a critical role to further reduce optical reflection in whole film structure. The wavelength-averaged reflectance of these samples is listed in Table 2. The whole oblique-aligned ZnO nanowires structure (grown at 265 °C) even shows significant suppression of reflectance of 87.5% and 90.0% for polished Si under TE and TM polarization, respectively, higher than the vertical-aligned nanowires. The mechanism of antireflection resulted from the grading reflective index of this structure. The effective refractive index of the ZnO oblique-aligned nanowire arrays, with subwavelength diameters, is larger than that of air and smaller than that of vertical-aligned nanowires, ZnO columns, buffer film, and Si substrate.[21,22,31,32] This is because the effective layer of the oblique-aligned ZnO nanowire arrays consists of multilayers of ZnO and air along the surface normal.

In Figure 5a and b, for polished Si, the wavelength-dependent reflectance for TM polarization is similar to and slightly lower than that for TE polarization, owing to the occurrence of the Brewster angle for TM. For the oscillated spectra of the oblique-aligned ZnO nanowires grown on 265 °C columns, the extremes obtained from the interference fringes for TE and TM polarization do not locate at the same wavelength position. This leads to the fact that in some wavelength regions the TE-mode reflectance of the oblique-aligned ZnO nanowires grown on 265 °C columns is slightly lower than its TM-mode reflectance, which is unusual

compared to the nature of the bulk Si at incident angles smaller than the Brewster angle. On the contrary, for the spectra of the oblique-aligned ZnO nanowires grown on 320 °C columns, there is no shift in the extremes of interference fringes for TE and TM polarization. This phenomenon can be elucidated as follows. The oblique-aligned ZnO nanowires grown on 265 °C columns with narrower and larger angle range of nanowires (60°−85°) are more optically anisotropic than those at 320 °C with broader and smaller angle range (30°−70°), leading to different reflectance fringes of the ZnO nanowires grown on 265 °C columns for TE and TM polarization.

We have demonstrated a novel defect-induced bending mechanism for a modified OAD system, where different defect density was introduced to accommodate the mass difference between the shadowed and exposed surfaces, leading to continuously structural bending without forming common planar defects, such as grain boundary, stacking fault, and twin. The columns gradually bent into opposite quadrants from the incident source, far from earlier OAD results. The curvature of column tips could be controlled by growth temperature, and in turn control the oblique direction of the nucleation and growth of the ZnO nanowire array in the second stage. The nanowire direction can be grown forward or backward relative to the incident flux determined by column tip curvature and neighboring column confinement. Ultimately, we demonstrate successful growth of a single crystal oblique-aligned ZnO nanowire array on bent ZnO columns with oblique-angle sputtering followed by a hydrothermal process. In principle, this growth mechanism is universal and can be applied to other materials. The significant advantages of the whole oblique-aligned ZnO nanowire structure applied in ARCs in terms of broad-band characteristics show the significant suppression of reflectance of 87.5% and 90.0% for polished Si under TE and TM polarization, respectively. In addition, the observed AR characteristics can be correlated with the structural properties instead of band-gap absorption. The interference oscillations of reflectance resulting from the effects of Fabry−Pérot cavities demonstrate that the optical anisotropy of the oblique-aligned ZnO nanowire arrays is dependent on the angle range of the nanowire direction.

Acknowledgment. This research was financially supported by the National Science Council (95-2221-E-006-080-MY3) of Taiwan and NCKU Landmark Project B015. The authors would like to thank the Center for Micro/Nano Science and Technology, National Cheng Kung University, Tainan, Taiwan, for equipment access and technical support, and also the NSC Core Facilities Laboratory for Nano-Science and Nano-Technology in the Kaohsiung-Pintung Area.

Supporting Information Available: SEM and HRTEM images, XRD spectra, and sketches showing the allowed growth directions of ZnO. This material is available free of charge via the Internet at http://pubs.acs.org.

References

(1) Knorr, T. G.; Hoffmann, R. W. *Phys. Rev.* **1959**, *113*, 1039.
(2) Smith, D. O. *J. Appl. Phys.* **1959**, *30*, 264S.
(3) Robbie, K.; Brett, M. J.; Lakhtakia, A. *Nature* **1996**, *384*, 616.
(4) Robbie, K.; Brett, M. J.; Lakhtakia, A. *J. Vac. Sci. Technol. A* **1995**, *13*, 2991.
(5) Dick, B.; Brett, M. J.; Smy, T. *J. Vac. Sci. Technol. B* **2003**, *21*, 2569.
(6) Robbie, K.; Sit, J. C.; Brett, M. J. *J. Vac. Sci. Technol. B* **1998**, *16*, 1115.
(7) Zhao, Y. P.; Ye, D. X.; Wang, G. C.; Lu, T. M. *Nano Lett.* **2002**, *2*, 351.
(8) Li, H. F.; Kar, A. K.; Parker, T.; Wang, G. C.; Lu, T. M. *Nanotechnology* **2008**, *19*, 335708.
(9) Kesapragada, S. V.; Gall, D. *Appl. Phys. Lett.* **2006**, *89*, 203121.
(10) Zhou, C. M.; Gall, D. *Appl. Phys. Lett.* **2006**, *88*, 203117.
(11) He, Y. P.; Zhao, Y. P.; Wu, J. S. *Appl. Phys. Lett.* **2008**, *92*, 063107.
(12) Tang, X. J.; Zhang, G.; Zhao, Y. P. *Nanotechnology* **2006**, *17*, 4439.
(13) Kesapragada, S. V.; Victor, P.; Nalamasu, O.; Gall, D. *Nano Lett.* **2006**, *6*, 854.
(14) Fu, J. X.; Collins, A.; Zhao, Y. P. *J. Phys. Chem. C* **2008**, *112*, 16784.
(15) He, Y. P.; Wu, J. S.; Zhao, Y. P. *Nano Lett.* **2007**, *7*, 1369.
(16) Singh, J. P.; Tang, F.; Karabacak, T.; Lu, T. M.; Wang, G. C. *J. Vac. Sci. Technol. B* **2004**, *22*, 1048.
(17) Summers, M. A.; Brett, M. J. *Nanotechnology* **2008**, *19*, 415203.
(18) Kennedy, S. R.; Brett, M. J. *J. Vac. Sci. Technol. B* **2004**, *22*, 1184.
(19) Xiao, X. D.; Dong, G. P.; Fan, Z. X.; Yi, K.; He, H. B.; Shao, J. D. *J. Phys. D: Appl. Phys.* **2009**, *42*, 165305.
(20) Saxena, K.; Mehta, D. S.; Srivastava, R.; Kamalasanan, M. N. *J. Phys. D: Appl. Phys.* **2008**, *41*, 015102.
(21) Chang, C. H.; Yu, P. C.; Yang, C. S. *Appl. Phys. Lett.* **2009**, *94*, 051114.
(22) Yu, P. C.; Chang, C. H.; Chiu, C. H.; Yang, C. S.; Yu, J. C.; Kuo, H. C.; Hsu, S. H.; Chang, Y. C. *Adv. Mater.* **2009**, *21*, 1618.
(23) Vick, D.; Friedrich, L. J.; Dew, S. K.; Brett, M. J.; Robbie, K.; Seto, M.; Smy, T. *Thin Solid Films* **1999**, *339*, 88.
(24) Abelmann, L.; Lodder, C. *Thin Solid Films* **1997**, *305*, 1.
(25) Hodgkinson, I. J.; Wu, Q. H.; Hazel, J. *Appl. Opt.* **1998**, *37*, 2653.
(26) Tait, R. N.; Smy, T.; Brett, M. J. *Thin Solid Films* **1993**, *226*, 196.
(27) Choi, W. K.; Li, L.; Chew, H. G.; Zheng, F. *Nanotechnology* **2007**, *18*, 385302.
(28) Teki, R.; Parker, T. C.; Li, H. F.; Koratkar, N.; Lu, T. M.; Lee, S. *Thin Solid Films* **2008**, *516*, 4993.
(29) Xi, J. Q.; Schubert, M. F.; Kim, J. K.; Schubert, E. F.; Chen, M.; Lin, S. Y.; Liu, W.; Smart, J. A. *Nature Photonics* **2007**, *1*, 176.
(30) Lee, Y. J.; Ruby, D. S.; Peters, D. W.; McKenzie, B. B.; Hsu, J. W. P. *Nano Lett.* **2008**, *8*, 1501.
(31) Huang, Y.-F.; Chattopadhyay, S.; Jen, Y.-J.; Peng, C.-Y.; Liu, T.-A.; Hsu, Y.-K.; Pan, C.-L.; Lo, H.-C.; Hsu, C.-H.; Chang, Y.-H.; Lee, C.-S.; Chen, K.-H.; Chen, L.-C. *Nat. Nanotechnol.* **2007**, *2*, 770.
(32) Bae, B.-J.; Hong, S.-H.; Hong, E.-J.; Lee, H.; Jung, G.-Y. *Jpn. J. Appl. Phys.* **2009**, *48*, 010207.